Supporting information for: Photoelectron Spectrum and Energetics of the meta-Xylylene Diradical

Mathias Steglich,[†] Victoria B. F. Custodis,[‡] Adam J. Trevitt,[¶] Gabriel daSilva,[§] Andras Bodi,[†] and Patrick Hemberger*[,†]

†*Paul Scherrer Institute, CH-5232 Villigen-PSI, Switzerland*
‡*Department of Chemistry and Applied Biosciences, Institute for Chemical and Bioengineering, ETH Zurich, HCI D 130, Vladimir-Prelog-Weg 1, 8093 Zurich, Switzerland*
¶*School of Chemistry, University of Wollongong, New South Wales 2522, Australia*
§*Department of Chemical and Biomolecular Engineering, The University of Melbourne, Victoria 3010, Australia*

E-mail: patrick.hemberger@psi.ch

Experimental methods

Experiments were carried out at the photoelectron photoion coincidence (PEPICO) endstation of the VUV beamline at the Swiss Light Source. Detailed descriptions of the beamline and the iPEPICO endstation are available elsewhere.[S1–S3] Synchrotron radiation was collimated, dispersed by a 150 mm^{-1} grating in grazing incidence and focused at the exit slit, achieving an energy resolution of 5 meV at 8 eV. A differentially pumped noble gas filter (10 mbar; Ar:Ne:Kr=3:6:1) absorbs higher diffraction orders, and the second order free VUV beam enters the PEPICO setup.

Flash vacuum pyrolysis of m-$C_8H_8I_2$. The synthesized *m*-$C_8H_8I_2$ precursor[S4] was heated to 70°C and, together with 300 mbar Ar buffer gas, expanded through a 100 μm pinhole into a resistively heated SiC tubular reactor. The reactor temperature of about (900 ± 100) K, as measured with a thermocouple, was optimized to give a strong signal in the mass spectrum at $m/z = 104$, while keeping fragment peaks at lower masses at a minimum. The molecular beam formed at the reactor exit was skimmed before entering the ionization region.

Photoelectron spectroscopy. The PEPICO setup enables velocity map imaging of the electrons and time-of-flight mass spectrometry of the ions. A constant field of 125 V / cm^{-1} accelerated the electrons towards a velocity map imaging delay-line detector and ions into a TOF mass spectrometer. Detected events were correlated in real-time in a multiple start/multiple stop scheme.[S5] Threshold electrons were selected with a resolution of 5 meV by selecting only the central part of the PE image. The hot electron background was subtracted as described elsewhere.[S6] ms-TPE spectra were acquired by scanning the photon energy in steps of 5 meV. The PE image was captured at a fixed photon energy of 7.8 eV and analyzed using one-dimensional projections of spherical functions.[S7] All energies were calibrated using known Ar lines. In the DPI experiment, *m*-$C_8H_8I_2$ was effusively expanded at room temperature and probed directly by VUV light to measure its ionization energy and investigate the dissociative photoionization. The breakdown diagram was modeled using statistical rate theory.[S8] All quantum chemical calculations were performed using the Gaussian09[S9] and the Q-Chem[S10] software packages. Franck-

Condon simulations were realized with Gaussian09 and ezSpectrum.[S11]

Determination of appearance energies

The breakdown diagram of 1,3-bis-iodomethyl benzene in Figure S1 depicts the fractional abundance of the parent and daughter ions in threshold photoionization as a function of photon energy, and is based on the photoion mass-selected threshold photoelectron signal. The fragmentation starts at around 8.7 eV with the first C–I bond dissociation and reaches 100% conversion to m-$C_8H_8I^+$ at 9.2 eV. The second consecutive iodine loss sets in at 11 eV and leads to m-xylylene ions.

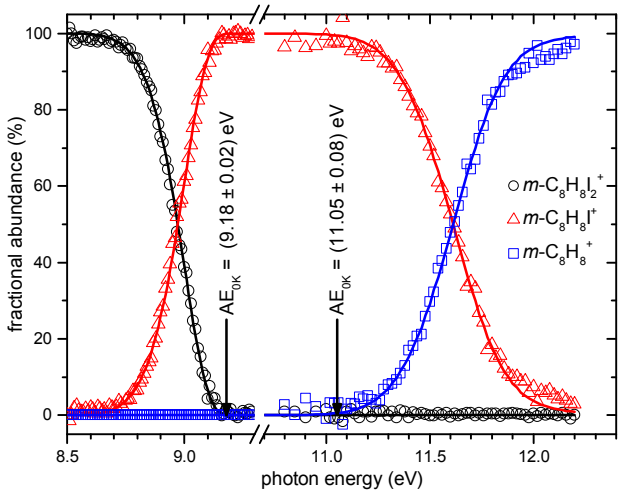

Figure S1: Breakdown diagram of 1,3-bis-iodomethyl benzene. The determined appearance energies ($AE_{0\,K}$) of both iodine losses are indicated.

In order to determine the appearance energies ($AE_{0\,K}$) accurately,[S8] the breakdown diagram and the time-of-flight distributions have to be modeled by taking into account the room temperature thermal energy distribution of the neutral, which is shifted into the ion's manifold, and is also available for fragmentation of the cation. This determines the breakdown diagram of the the first C–I bond breaking, which is a fast process, as evidenced by the symmetric daughter ion peaks shapes and is not affected by a kinetic shift. Thus, the only adjustable parameter is the 0 K appearance energy, which was optimized to 9.18 ± 0.02 eV. Illustrative experimental time-of-flight distributions are depicted in Figure S2 along with the modeled ones and the goodness of the fit. The latter was obtained by scanning the barrier and evaluating the quality of the fit, yielding a ±20 meV confidence interval for our model. The long first acceleration stage of the iPEPICO spectrometer allows us to measure rate constants in a $10^3 < k / s^{-1} < 10^7$ range (see Figure S2, bottom trace), and employ statistical theories to extrapolate the rate curve to the threshold. While the first fragment ion appears in the mass spectrum in the form of symmetric time-of-flight distributions (Figure S2, upper trace), indicative of fast dissociation rates above $k > 10^7$, the second C–I bond breaking is affected by a kinetic shift (Figure S2, middle trace).

In order to model the second step, the excess energy above the dissociation barrier is first distributed statistically to evaluate the internal energy distribution of the intermediate $C_8H_8I^+$ fragment ion.[S12] Since this medium-sized ion possesses numerous internal degrees of freedom, and is quite stable, it is not surprising that it dissociates slowly close to the thermochemical threshold of the iodine loss. This so-called kinetic effect shifts the breakdown diagram to the blue and leads to asymmetric time-of-flight distributions, indicative of metastable parent ions. The thermochemical onset of a slow dissociation reaction is found were the rates vanish, which makes it necessary to use statistical theories to extrapolate the experimental rates. Because it was shown to perform well in similar halogen atom loss reactions, we used the simplified statistical adiabatic channel model (SSACM), which can be thought of as a generalized version of phase space theory.[S13,S14]

The rate equation,

$$k(E) = \frac{\sigma N^{\ddagger}(E - \mathrm{AE}_0)}{h\rho(E)}, \qquad (1)$$

depends on $N^{\ddagger}$, the number of states of the transition state above the threshold AE_0, and on ρ, which is the density of states of the reac-

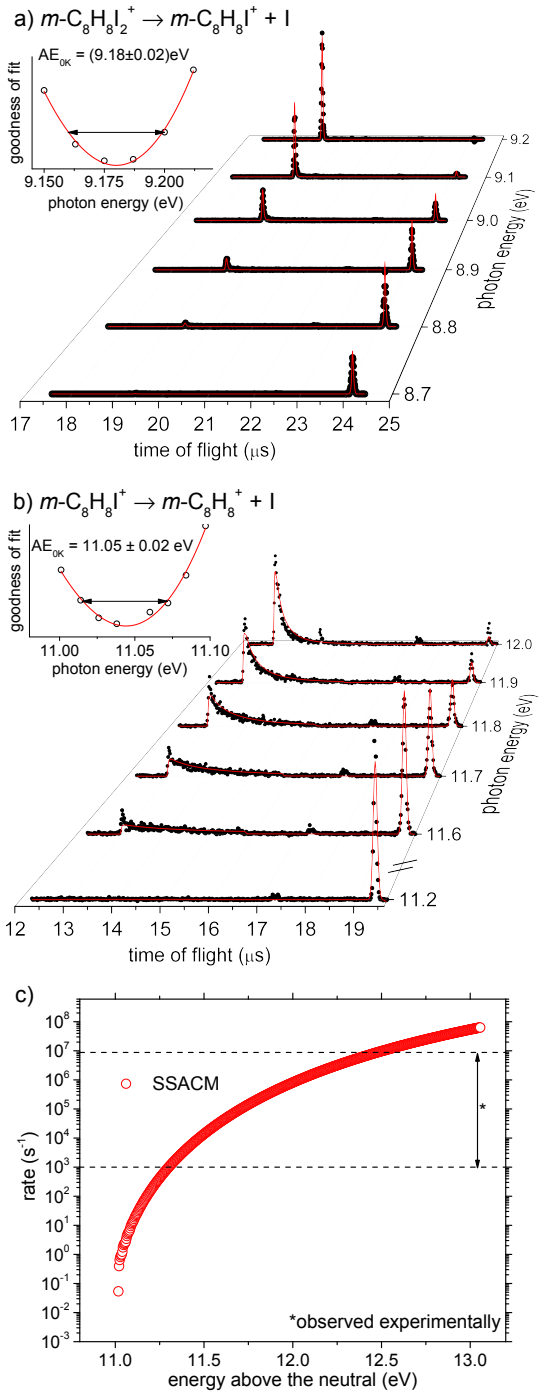

Figure S2: Time-of-flight distribution of the first (a) and second C-I bond dissociation (b) along with the error assessment of each reaction. (c) Rate curve of second iodine loss according to SSACM theory.

tant. In eq. 1, h is Planck's constant and σ is the symmetry number. Both the number and density of states are determined by state counting algorithms using harmonic frequencies obtained at the B3LYP/6-311++G(d,p) level of theory.

Similar to phase space theory, the transition state number of states is based on the products in SSACM. In the fit, the number of states is scaled by an energy-dependent rigidity factor to reproduce the experimentally measured dissociation rates:

$$f_{rigid} = \exp \frac{-(E - \mathrm{AE}_0)}{c} \qquad (2)$$

Parameter c in eq. 2 reflects the anisotropy of the potential and is the second fitting parameter in addition to the appearance energy. The developed model delivers an AE_{0K} of 11.05 eV. Although the fit is quite well defined, there may be systematic errors in the shape of the rate curve (Figure S2, bottom trace), which leads us to increase the error bar to 0.08 eV. We have used the miniPEPICO (Rev. 193) program in the statistical modeling of the iPEPICO data.[S8]

Formation enthalpy calculations

Since the formation enthalpy of 1,3-bis-iodomethyl benzene was not determined yet, and is needed to anchor our positive ion cycle to the standard thermochemical scale, we have used the isodesmic reaction displayed in Table S1 in order to determine this value. The calculated mean reaction enthalpy $(0.3 \pm 1)\,\mathrm{kJ\,mol^{-1}}$ together with the formation enthalpies of benzyliodide[S15] $(127.3 \pm 1.3)\,\mathrm{kJ\,mol^{-1}}$ and benzene[S16] $(82.9 \pm 0.9)\,\mathrm{kJ\,mol^{-1}}$ delivers a $\Delta H_{f,298\,\mathrm{K}}(m\text{-}\mathrm{C_8H_8I_2}) = 172.0\,\mathrm{kJ\,mol^{-1}}$. After shifting to 0 K (see eq. 3), using a thermal correction factor to the enthalpy (Table S1) along with elemental corrections, we end up at $198.6\,\mathrm{kJ\,mol^{-1}}$.[S17,S18]

$$\Delta H_{f,298\,\mathrm{K}} - \Delta H_{f,0\,\mathrm{K}} = (H_{298\,\mathrm{K}} - H_{0\,\mathrm{K}}) - \sum_{\text{constituent elements}} (H_{298\,\mathrm{K}} - H_{0\,\mathrm{K}}) \quad (3)$$

Both C–I bond dissociation reactions take place along purely attractive reaction energy curves with the fragmentation products corresponding to the maximum energy value, as confirmed by scanning the C–I bond length and relaxing the remaining coordinates in *ab initio* geometry optimizations. In addition, if there were a reverse barrier involved, a similarly higher $H_{f,298\,\mathrm{K}}(m\text{-}C_8H_8)$ would have been determined.

Table S1: Calculated heats of reaction for the formation of 1,3-bis-iodomethyl benzene and thermal correction factors to enthalpy given in $\mathrm{kJ\,mol^{-1}}$.

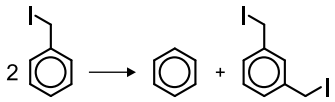

method	$\Delta H_{R,298\,\mathrm{K}}$	$H_{298\,\mathrm{K}} - H_{0\,\mathrm{K}}$
		m-$C_8H_8I_2$
B3LYP/6-311++G(d,p)	1.0	29.2
B3LYP/cc-pVTZ	1.0	29.0
MP2/6-311++G(d,p)	2.9	29.4
MP2/cc-pVTZ	−0.7	28.9
ωB97X-D/6-311++G(d,p)	−0.8	28.6
ωB97X-D/cc-pVTZ	−1.0	28.3
M06L/6-311++G(d,p)	0.2	29.0
M06L/cc-pVTZ	0.0	28.7
average	0.3 ± 1.0	28.9 ± 0.3
		C: 1.05[S17]
		H_2: 8.47[S17]
		I_2:13.198[S17]

To test the reliability of the calculated formation enthalpy of the precursor, we have evaluated our approach against known $\Delta H_{f,298\,\mathrm{K}}$ of ethyliodide and benzyliodide and found agreement within $2\,\mathrm{kJ\,mol^{-1}}$. The error bars of the computationally determined $\Delta H_{f,298\,\mathrm{K}}$ of m-$C_8H_8I_2$ are small compared to the conservatively set uncertainty of the model used to determine the appearance energy (0.08 eV; $8\,\mathrm{kJ\,mol^{-1}}$).

The thermal correction factors to the enthalpies of m-C_8H_8 are summarized in Table S2. Calculated reaction enthalpies, $\Delta H_{R,298\,\mathrm{K}}$ of eq. 4, 5, and 6, which were used to derive the $\Delta H_{f,298\,\mathrm{K}}$ are given in Table S3. We have used tabulated $\Delta H_{f,298\,\mathrm{K}}$ of m-xylene ($17.2\,\mathrm{kJ\,mol^{-1}}$), methylene ($391.52\,\mathrm{kJ\,mol^{-1}}$), methane ($-74.533\,\mathrm{kJ\,mol^{-1}}$) and methyl ($146.427\,\mathrm{kJ\,mol^{-1}}$).[S19]

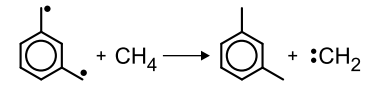

(4)

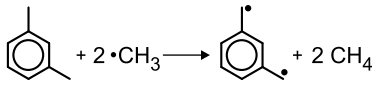

(5)

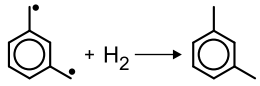

(6)

Table S2: Calculated thermal correction factors for m-C_8H_8 in $\mathrm{kJ\,mol^{-1}}$.

method	$H_{298\,\mathrm{K}} - H_{0\,\mathrm{K}}(m\text{-}C_8H_8)$
B3LYP/6-311++G(d,p)	18.3
B3LYP/cc-pVTZ	18.2
MP2/6-311++G(d,p)	18.7
MP2/cc-pVTZ	17.7
ωB97X-D/6-311++G(d,p)	18.3
ωB97X-D/cc-pVTZ	18.3
M06L/6-311++G(d,p)	18.5
M06L/cc-pVTZ	17.7
average	18.2 ± 0.4

Table S3: Calculated reaction enthalpies $\Delta H_{R,298\,\mathrm{K}}$ for m-C_8H_8 in $\mathrm{kJ\,mol^{-1}}$.

method	$\Delta H_{R,298\,\mathrm{K}}$		
	eq. 4	eq. 5	eq. 6
G4	154.6	−128.5	−308.5
CBS-QB3	162.4	−137.9	−303.3
CBS-APNO	160.4	−135.4	−308.7

Molecular orbital and charge densities

The precursor cation has a very low C–I bond energy of only 0.68 eV. The ionization of *m*-$C_8H_8I_2$ takes place from the π-electron system of the benzene moiety and from the iodine lone pair (see Fig. S3, HOMO of *m*-$C_8H_8I_2$), which induces a positive charge to be located also at the iodine atom (see electrostatic potentials in Fig. S3). Bond cleavage of the C–I bond leads to formation of the *m*-$C_8H_8I^+$ fragment, where the positive charge is almost exclusively located in the benzene moiety. This stabilization leads to the observed lowering of the bond energy.

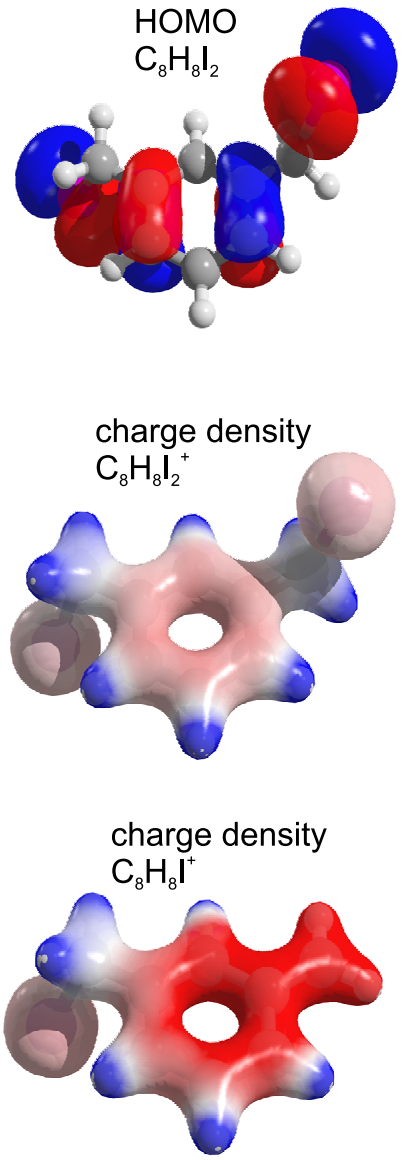

Figure S3: HOMO orbital of the neutral precursor and charge densities of the parent ($C_8H_8I_2^+$) and fragment ($C_8H_8I^+$) ions.

References

(S1) Bodi, A.; Johnson, M.; Gerber, T.; Gengeliczki, Z.; Sztáray, B.; Baer, T. *Rev. Sci. Instrum.* **2009**, *80*, 034101/1–034101/7.

(S2) Johnson, M.; Bodi, A.; Schulz, L.; Gerber, T. *Nucl. Instrum. Methods Phys. Res., Sect. A* **2009**, *610*, 597–603.

(S3) Bodi, A.; Hemberger, P.; Gerber, T.; Sztáray, B. *Rev. Sci. Instrum.* **2012**, *83*, 083105/1–083105/8.

(S4) T.Kida,; Kikuzawa, A.; Higashimoto, H.; Nakatsuji, Y.; Akashi, M. *Tetrahedron* **2005**, *61*, 5763–5768.

(S5) Bodi, A.; Sztáray, B.; Baer, T.; Johnson, M.; Gerber, T. *Rev. Sci. Instrum.* **2007**, *78*, 084102/1–084102/7.

(S6) Sztáray, B.; Baer, T. *Rev. Sci. Instrum.* **2003**, *74*, 3763–3768.

(S7) Gerber, T.; Liu, Y.; Knopp, G.; Hemberger, P.; Bodi, A.; Radiand, P.; Sych, Y. *Rev. Sci. Instrum.* **2013**, *84*, 033101/1–033101/10.

(S8) Sztáray, B.; Bodi, A.; Baer, T. *J. Mass Spectrom.* **2010**, *45*, 1233–1245.

(S9) Frisch, M. J.; Trucks, G. W.; Schlegel, H. B.; Scuseria, G. E.; Robb, M. A.; Cheeseman, J. R.; Scalmani, G.; Barone, V.; Mennucci, B.; Petersson, G. A.; Nakatsuji, H.; Caricato, M.; Li, X.; Hratchian, H. P.; Izmaylov, A. F.; Bloino, J.; Zheng, G.; Sonnenberg, J. L.; Hada, M.; Ehara, M.; Toyota, K.; Fukuda, R.; Hasegawa, J.; Ishida, M.; Nakajima, T.; Honda, Y.; Nakai, O. K. H.; Vreven, T.; Montgomery, J. A.; Peralta, J. E.; Ogliaro, F.; Bearpark, M.; Heyd, J. J.; Brothers, E.; Kudin, K. N.; Staroverov, V. N.; Keith, T.; Kobayashi, R.; Normand, J.; Raghavachari, K.; Rendell, A.; Burant, J. C.; Iyengar, S. S.; Tomasi, J.; Cossi, M.; Rega, N.; Millam, J. M.; Klene, M.; Knox, J. E.; Cross, J. B.; Bakken, V.; Adamo, C.; Jaramillo, J.; Gomperts, R.; Stratmann, R. E.; Yazyev, O.; Austin, A. J.; Cammi, R.; Pomelli, C.; Ochterski, J. W.; Martin, R. L.; Morokuma, K.; Zakrzewski, V. G.; Voth, G. A.; Salvador, P.; Dannenberg, J. J.; Dapprich, S.; Daniels, A. D.; Farkas, O.; Foresman, J. B.; Ortiz, J. V.; Cioslowski, J.; Fox, D. J. *Gaussian 09, Revision E.01*; 2013.

(S10) Shao, Y.; Gan, Z.; Epifanovsky, E.; Gilbert, A. T.; Wormit, M.; Kussmann, J.; Lange, A. W.; Behn, A.; Deng, J.; Feng, X.; Ghosh, D.; Goldey, M.; Horn, P. R.; Jacobson, L. D.; Kaliman, I.; Khaliullin, R. Z.; KuÅŻ, T.; Landau, A.; Liu, J.; Proynov, E. I.; Rhee, Y. M.; Richard, R. M.; Rohrdanz, M. A.; Steele, R. P.; Sundstrom, E. J.; III, H. L. W.; Zimmerman, P. M.; Zuev, D.; Albrecht, B.; Alguire, E.; Austin, B.; Beran, G. J. O.; Bernard, Y. A.; Berquist, E.; Brandhorst, K.; Bravaya, K. B.; Brown, S. T.; Casanova, D.; Chang, C.-M.; Chen, Y.; Chien, S. H.; Closser, K. D.; Crittenden, D. L.; Diedenhofen, M.; Jr., R. A. D.; Do, H.; Dutoi, A. D.; Edgar, R. G.; Fatehi, S.; Fusti-Molnar, L.; Ghysels, A.; Golubeva-Zadorozhnaya, A.; Gomes, J.; Hanson-Heine, M. W.; Harbach, P. H.; Hauser, A. W.; Hohenstein, E. G.; Holden, Z. C.; Jagau, T.-C.; Ji, H.; Kaduk, B.; Khistyaev, K.; Kim, J.; Kim, J.; King, R. A.; Klunzinger, P.; Kosenkov, D.; Kowalczyk, T.; Krauter, C. M.; Lao, K. U.; Laurent, A. D.; Lawler, K. V.; Levchenko, S. V.; Lin, C. Y.; Liu, F.; Livshits, E.; Lochan, R. C.; Luenser, A.; Manohar, P.; Manzer, S. F.; Mao, S.-P.; Mardirossian, N.; Marenich, A. V.; Maurer, S. A.; Mayhall, N. J.; Neuscamman, E.; Oana, C. M.; Olivares-Amaya, R.; OâĂŹNeill, D. P.; Parkhill, J. A.; Perrine, T. M.; Peverati, R.; Prociuk, A.; Rehn, D. R.; Rosta, E.; Russ, N. J.; Sharada, S. M.; Sharma, S.; Small, D. W.; Sodt, A.; Stein, T.; StÃijck, D.; Su, Y.-C.; Thom, A. J.; Tsuchimochi, T.; Vanovschi, V.; Vogt, L.; Vydrov, O.; Wang, T.; Watson, M. A.; Wenzel, J.; White, A.; Williams, C. F.; Yang, J.; Yeganeh, S.; Yost, S. R.; You, Z.-Q.; Zhang, I. Y.; Zhang, X.; Zhao, Y.; Brooks, B. R.; Chan, G. K.; Chipman, D. M.; Cramer, C. J.; III, W. A. G.; Gordon, M. S.; Hehre, W. J.; Klamt, A.; III, H. F. S.; Schmidt, M. W.; Sherrill, C. D.; Truhlar, D. G.; Warshel, A.; Xu, X.; Aspuru-Guzik, A.; Baer, R.; Bell, A. T.; Besley, N. A.; Chai, J.-D.; Dreuw, A.; Dunietz, B. D.; Furlani, T. R.; Gwaltney, S. R.; Hsu, C.-P.; Jung, Y.; Kong, J.; Lambrecht, D. S.; Liang, W.; Ochsenfeld, C.; Rassolov, V. A.; Slipchenko, L. V.; Subotnik, J. E.; Voorhis, T. V.; Herbert, J. M.; Krylov, A. I.; Gill, P. M.; Head-Gordon, M. *Molecular Physics* **2015**, *113*, 184–215.

(S11) Mozhayskiy, V. A.; Krylov, A. I. ezSpectrum. http://iopenshell.usc.edu/downloads.

(S12) Sztáray, B.; Baer, T. *J. Phys. Chem. A* **2002**, *106*, 8046–8053.

(S13) Stevens, W.; Sztáray, B.; Shuman, N.; Baer, T.; Jürgen, T. *J. Phys. Chem. A* **2009**, *113*, 573–582.

(S14) Troe, J.; Ushakov, V. G.; Viggiano, A. A. *J. Phys. Chem. A* **2006**, *110*, 1491–1499.

(S15) Walsh, R.; Golden, D. M.; Benson, S. W. *J. Am. Chem. Soc.* **1966**, *88*, 650–656.

(S16) Roux, M. V.; Temprado, M.; Chickos, J. S.; Nagano, Y. *J. Phys. Chem. Ref. Data* **2008**, *37*, 1855–1996.

(S17) Chase, M. W. *J. Phys. Chem. Ref. Data, Monogr.* **1998**, *9*, 1–1963.

(S18) Harvey, J.; Bodi, A.; Tuckett, R. P.; Sztáray, B. *Phys. Chem. Chem. Phys.* **2012**, *14*, 3935–3948.

(S19) Ruscic, B. *Active Thermochemical Tables* **2013**, *values based on ver. 1.119 of the Thermochemical Network*, available at ATcT.anl.gov.